12

Surface plasmons

The interaction of metals with electromagnetic radiation is largely dictated by the free conduction electrons in the metal. According to the simple Drude model, the free electrons oscillate 180° out of phase relative to the driving electric field. As a consequence, most metals possess a negative dielectric constant at optical frequencies which causes, for example, a very high reflectivity. Furthermore, at optical frequencies the metal's free electron gas can sustain surface and volume charge density oscillations, called plasmon polaritons or plasmons with distinct resonance frequencies. The existence of plasmons is characteristic of the interaction of metal nanostructures with light. Similar behavior cannot be simply reproduced in other spectral ranges using the scale invariance of Maxwell's equations since the material parameters change considerably with frequency. Specifically, this means that model experiments with, for instance, microwaves and correspondingly larger metal structures cannot replace experiments with metal nanostructures at optical frequencies. The surface charge density oscillations associated with surface plasmons at the interface between a metal and a dielectric can give rise to strongly enhanced optical near-fields which are spatially confined near the metal surface. Similarly, if the electron gas is confined in three dimensions, as in the case of a small subwavelength-scale particle, the overall displacement of the electrons with respect to the positively charged lattice leads to a restoring force, which in turn gives rise to specific particle-plasmon resonances depending on the geometry of the particle. In particles of suitable (usually pointed) shape, extreme local charge accumulations can occur that are accompanied by strongly enhanced optical fields.

The study of optical phenomena related to the electromagnetic response of metals has been recently termed *plasmonics* or *nanoplasmonics*. This rapidly growing field of nanoscience is mostly concerned with the control of optical radiation on the subwavelength scale. Many innovative concepts and applications of metal optics have been developed over the past few years and in this chapter we discuss a few examples. Since most of the physics of the interaction of light with metal

away from the interface can be obtained from (12.18) to first order in $|\varepsilon_1''| / |\varepsilon_1'|$ using (12.21) as

$$k_{1,z} = \frac{\omega}{c}\sqrt{\frac{\varepsilon_1'^2}{\varepsilon_1' + \varepsilon_2}}\left[1 + \mathrm{i}\frac{\varepsilon_1''}{2\varepsilon_1'}\right], \tag{12.25}$$

$$k_{2,z} = \frac{\omega}{c}\sqrt{\frac{\varepsilon_2^2}{\varepsilon_1' + \varepsilon_2}}\left[1 - \mathrm{i}\frac{\varepsilon_1''}{2(\varepsilon_1' + \varepsilon_2)}\right]. \tag{12.26}$$

Using the same parameters for silver and gold as before and safely neglecting the very small imaginary parts we obtain for the 1/e decay lengths pairs $(1/k_{1,z}, 1/k_{2,z})$ of the electric fields (23 nm, 421 nm) and (28 nm, 328 nm), respectively. This shows that the decay into the metal is much shorter than into the dielectric. It also shows that a sizable amount of the SPP electric field can reach through a thin enough metal film. The decay of the SPP into the air half-space was observed directly in [9] using a scanning tunneling optical microscope.

An important parameter is the intensity enhancement near the interface due to the excitation of surface plasmons. This parameter can be obtained by evaluating the ratio of the incoming intensity and the intensity right above the metal interface. We skip this discussion for the moment and come back to it after the next section (see Problem 12.4). However, we note that losses in the plasmon's propagation were directly derived from the metal's bulk dielectric function. This is a good approximation as long as the characteristic dimensions of the considered metal structures are larger than the electron mean-free path. If the dimensions become smaller, there is an increasing chance of electron scattering from the interface. In other words, close to the interface additional loss mechanisms have to be taken into account that locally increase the imaginary part of the metal's dielectric function. It is difficult to correctly account for these so-called non-local losses as the exact parameters are not known. Nevertheless, since the fields associated with surface plasmons penetrate into the metal by more than 10 nm the non-local effects associated with the first few atomic layers can be safely ignored.

12.2.2 Excitation of surface plasmon polaritons

In order to excite surface plasmon polaritons we have to fulfil both energy and momentum conservation. To see how this can be done we have to analyze the dispersion relation of the surface waves, i.e. the relation between energy in terms of the angular frequency ω and the momentum in terms of the wavevector in the propagation direction k_x given by Eq. (12.17) and Eq. (12.22). In order to plot this dispersion relation we assume that ε_1 is real, positive, and independent of ω, which is true for e.g. air ($\varepsilon_1 = 1$).

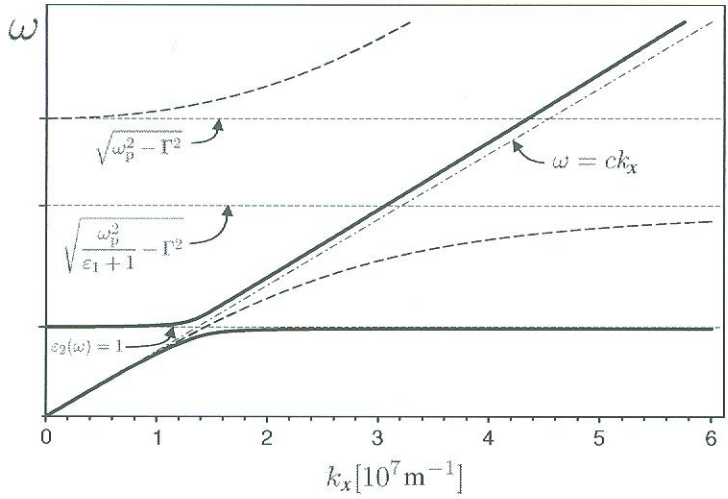

Figure 12.5 Dispersion relation of surface plasmon polaritons at a gold/air interface. The solid line is the dispersion relation that results from a dielectric function accounting for a single interband transition. The dashed line results from using a Drude type dielectric function. The dash-dotted straight line is the light line $\omega = c \cdot k_x$ in air.

For the metal we discuss two cases: (i) the pure Drude–Sommerfeld dielectric function given by (12.6) and (ii) the more realistic dielectric function that includes an interband transition (12.9). For both cases only the real part of $\varepsilon_2(\omega)$ is considered, neglecting the damping of the surface wave in the x-direction. Figure 12.5 shows the respective plots. The solid line is the dispersion relation for the more realistic metal. The thick dashed line is the corresponding dispersion relation when interband transition effects are neglected, i.e. for a pure Drude metal. The dash-dotted line is the light line $\omega = c \cdot k_x$ in air and the horizontal thin dashed lines mark important values of ω. For large k_x the simple Drude description results in a dispersion relation that clearly differs from the more realistic case, although the main features are similar. The dispersion relation shows two branches, a high-energy and a low-energy branch. The high-energy branch, called the Brewster mode, does not describe true surface waves, since according to (12.18) the z-component of the wavevector in the metal is no longer purely imaginary. This branch will not be considered further. The low-energy branch corresponds to a true interface wave, the surface plasmon polariton. The annex polariton is used to highlight the intimate coupling between the charge density wave on the metal surface (surface plasmon) and the light field in the dielectric medium (photon).

For completeness we need to mention that if damping is taken fully into account there is a continuous transition from the surface plasmon dispersion in Fig. 12.5

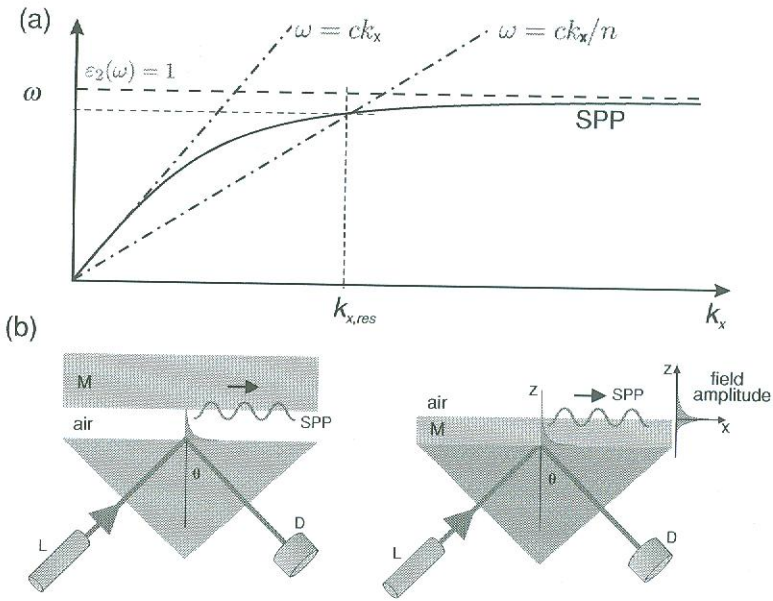

Figure 12.6 Excitation of surface plasmons. (a) Close-up of the dispersion relation with the free-space light line and the tilted light line in glass. (b) Experimental arrangements to realize the condition sketched in (a). Left: Otto configuration. Right: Kretschmann configuration. L: laser, D: detector, M: metal layer.

into the upper high-energy branch. If we follow the dispersion curve in Fig. 12.5 starting from $\omega = 0$ then we first move continuously from the light line towards the horizontal line determined by the surface plasmon resonance condition $\varepsilon_2(\omega) = 1$. However, as the dispersion curve approaches this line the losses start to increase drastically. As a consequence, as ω is further increased the dispersion curve bends back and connects to the upper branch. In the connecting region the energy of the mode is strongly localized inside the metal, which explains the high losses. The backbending effect has been experimentally verified (see Ref. [10]) and poses a limit to the maximum wavenumber k_x that can be achieved in an experiment. Usually, this maximum k_x is smaller than $\approx 3\omega/c$.

An important feature of surface plasmons is that for a given energy $\hbar\omega$ the wavevector k_x is always larger than the wavevector of light in free space. This is obvious by inspecting (12.17) and also from Fig. 12.5 and Fig. 12.6(a) where the light line ω/c is plotted as a dash-dotted line. This light line is asymptotically approached by the SPP dispersion for small energies. The physical reason for the increased momentum of the SPP is the strong coupling between light and surface charges. The light field has to "drag" the electrons along the metal surface. Consequently, this means that a SPP on a plane interface cannot be excited by light of any frequency that propagates in free space. Excitation of a SPP by light is only

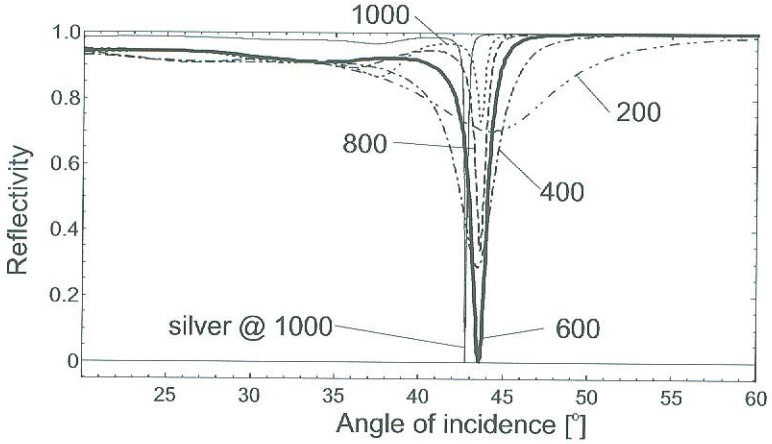

Figure 12.7 Excitation of surface plasmons in the Otto configuration. The reflectivity of the exciting beam is plotted as a function of the incident angle and for different air gaps (in nm). The curves are evaluated for a gold film. For comparison, a single trace is also plotted for silver for which the resonance is much sharper because of lower damping.

possible if a wavevector component of the exciting light can be increased over its free-space value. There are several ways to achieve this increase of the wavevector component. The conceptually most simple solution is to excite surface plasmons by means of evanescent waves created at the interface between a medium with refractive index $n > 1$. The light line in this case is tilted by a factor of n since $\omega = ck/n$. This situation is shown in Fig. 12.6(a), which shows the SPP dispersion with the free-space light line and the tilted light line in glass.

Figure 12.6(b) shows a sketch of the possible experimental arrangements that realize this idea. In the Otto configuration [11] the tail of an evanescent wave at a glass/air interface is brought into contact with a metal/air interface that supports SPPs. For a sufficiently large separation between the two interfaces (gapwidth) the evanescent wave is only weakly influenced by the presence of the metal. By tuning the angle of incidence of the totally reflected beam inside the prism, the resonance condition for excitation of SPPs, i.e. the matching of the parallel wavevector components, can be fulfilled. The excitation of a SPP will show up as a minimum in the reflected light. The reflectivity of the system as a function of the angle of incidence and of the gapwidth is shown in Fig. 12.7. For the angle of incidence a clear resonance is observed at 43.5°. For a small gapwidth the resonance is broadened and shifted due to radiation damping of the SPP. This is caused by the presence of the glass half-space, which allows the SPP to rapidly decay radiatively by transforming the evanescent SPP field into a propagating field in the glass. For a gapwidth that is too large the SPP can no longer be efficiently excited and the resonance vanishes.

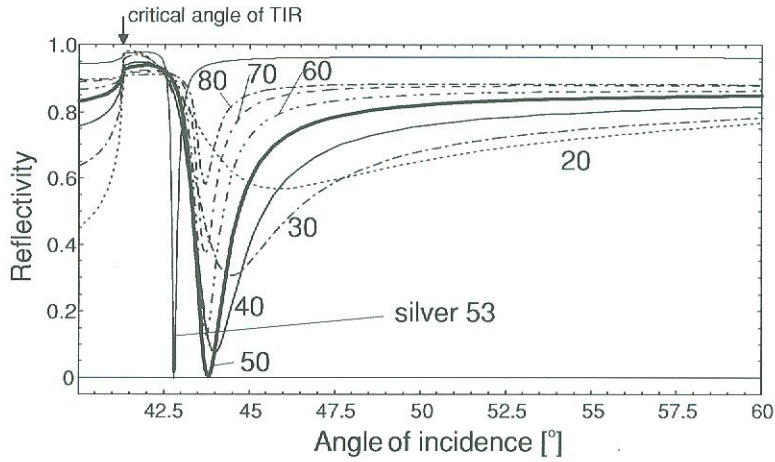

Figure 12.8 Excitation of surface plasmons in the Kretschmann configuration. The reflectivity of the exciting beam is plotted as a function of the incident angle and for different thicknesses of a gold film on glass (in nm). For comparison a single trace is plotted for a silver film. Note the much sharper resonance due to the smaller damping of silver as compared to gold. The critical angle of total internal reflection shows up as a discontinuity marked by an arrow.

The Otto configuration proved to be experimentally inconvenient because of the challenging control of the tiny air gap between the two interfaces. In 1971 Kretschmann came up with an alternative method to excite SPP that solved this problem [12]. In his method, a thin metal film is deposited on top of a prism. The geometry is sketched in Fig. 12.6(b). To excite a surface plasmon at the metal/air interface an evanescent wave created at the glass/metal interface has to penetrate through the metal layer. Here, similar arguments apply as for the Otto configuration. If the metal is too thin, the SPP will be strongly damped because of radiation damping into the glass. If the metal film is too thick the SPP can no longer be efficiently excited due to absorption in the metal. Figure 12.8 shows the reflectivity of the excitation beam as a function of the metal film thickness and the angle of incidence. As before, the resonant excitation of surface plasmons is characterized by a dip in the reflectivity curves.

It is worth mentioning that for the occurrence of a minimum in the reflectivity curves in both the Otto and the Kretschmann configurations at least two (equivalent) physical interpretations can be given. The first interpretation is that the minimum can be thought of as being due to destructive interference between the totally reflected light and the light emitted by the SPP due to radiation damping. In the second interpretation, the missing light is assumed to have been totally converted to surface plasmons at the interface which carry away the energy along the interface so that it cannot reach the detector.

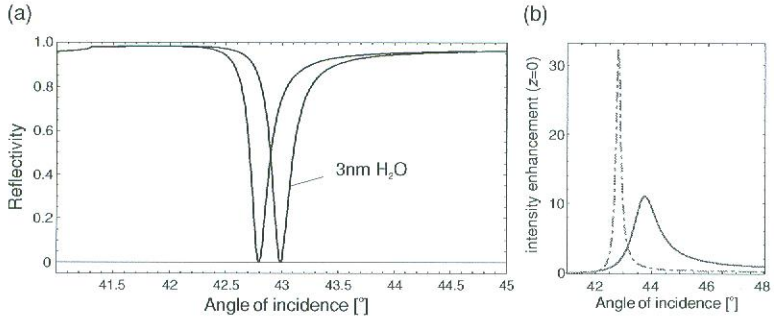

Figure 12.9 Surface plasmons used in sensor applications. (a) Calculated shift of the SPP resonance curve induced by a 3 nm layer of water ($n = 1.33$) adsorbed on a 53 nm silver film. (b) Intensity enhancement near the metal surface as a function of the angle of incidence in the Kretschmann configuration. For silver ($\varepsilon_1 = -18.2 + 0.5$i, dash-dotted line) and gold ($\varepsilon_1 = -11.6 + 1.2$i, solid line) at a wavelength of 633 nm we observe a maximum intensity enhancement of ~32 and ~10, respectively.

An alternative way to excite SPP is the use of a grating coupler [8]. Here, the increase of the wavevector necessary to match the SPP momentum is achieved by adding a reciprocal lattice vector of the grating to the free-space wavevector. This requires in principle that the metal surface is structured with the right periodicity a over an extended spatial region. The new parallel wavevector then reads as $k'_x = k_x + 2\pi n/a$ with $2\pi n/a$ being a reciprocal lattice vector. A recent prominent application of this SPP excitation principle was used to enhance the interaction of subwavelength holes with SPP in silver films [13].

12.2.3 Surface plasmon sensors

The distinct resonance condition associated with the excitation of surface plasmons has found application in various sensors. For example, the position of the dip in the reflectivity curves can be used as an indicator for environmental changes. With this method, the adsorption or removal of target materials on the metal surface can be detected with submonolayer accuracy. Figure 12.9 illustrates this capability by a simulation. It shows the effect of a 3 nm layer of water on top of a 53 nm thick silver film on glass. A strongly shifted plasmon resonance curve can be observed. Assuming that the angle of incidence of the excitation beam has been adjusted to the dip in the reflectivity curve, the deposition of a minute amount of material increases the signal (reflectivity) drastically. This means that the full dynamic range of a low-noise intensity measurement can be used to measure a coverage ranging between 0 and 3 nm. Consequently, SPP sensors are very attractive for applications ranging from biological binding assays to environmental sensing. For reviews see e.g. [14, 15].

The reason for the extreme sensitivity lies in the fact that the light intensity near the metal surface is strongly enhanced. In the Kretschmann configuration, this enhancement factor can be determined by evaluating the ratio of the intensity above the metal and the incoming intensity. In Fig. 12.9(b) this ratio is calculated and plotted as a function of the angle of incidence for both gold and silver for a 50 nm thin film. Clear resonant behavior is again observed which reflects the presence of the SPP.

12.3 Surface plasmons in nano-optics

Scanning near-field optical microscopy as well as fluorescence studies lead to new ways of exciting SPP [16, 18, 19]. The parallel components of the wavevector (k_x) necessary for SPP excitation are also present in confined optical near-fields in the vicinity of subwavelength apertures, metallic particles or even fluorescent molecules. If such confined fields are brought close enough to a metal surface, coupling to SPP can be accomplished *locally*. Figure 12.10 shows the principal arrangements. A metal film resides on a (hemispherical) glass prism to allow light (e.g. due to radiation damping of the SPP) to escape and to be recorded. In order to excite surface plasmons, the exciting light field needs to have evanescent field components that match the parallel wavevector k_x of the surface plasmon. As an illustration, Fig. 12.11(a) shows the excitation of surface plasmons with an oscillating dipole placed near the surface of a thin silver film deposited on a glass surface. The figure depicts contour lines of constant power density evaluated at a certain instant of time and displayed on a logarithmic scale. The surface plasmons propagating on the top surface decay radiatively as seen by the wavefronts in the lower medium. The situation is reciprocal to the situation of the Kretschmann configuration discussed earlier where such radiation is used to excite surface plasmons. Also

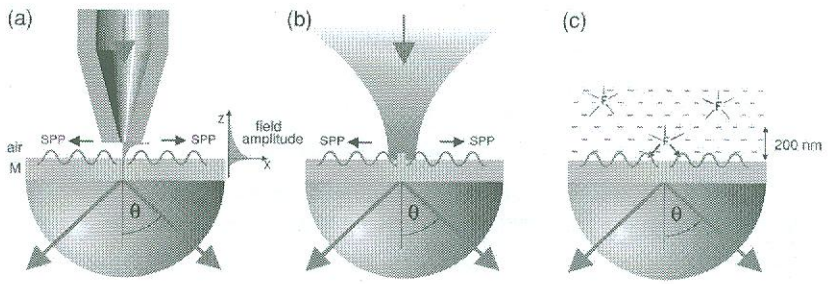

Figure 12.10 Local excitation of surface plasmons on a metal film with different confined light fields. (a) A subwavelength light source such as an aperture probe [16], (b) an irradiated nanoparticle [17], and (c) fluorescent molecules [18]. In all cases, surface plasmons are excited by evanescent field components that match the parallel wavevector k_x of the surface plasmon.

structures is hidden in the frequency dependence of the metal's complex dielectric function, we begin with a discussion of the fundamental optical properties of metals. We then turn to important solutions of Maxwell's equations for noble metal structures, i.e. the plane metal–dielectric interface and subwavelength metallic wires and particles that show resonant behavior. Where appropriate, applications of surface plasmons in nano-optics are discussed. As *nanoplasmonics* is a very active field of study we can expect that many new applications will be developed in the years to come and that dedicated texts will be published. Finally, it should be noted that optical interactions similar to those discussed here are also encountered for infrared radiation interacting with polar materials. The corresponding excitations are called surface phonon polaritons.

12.1 Optical properties of noble metals

The optical properties of metals and noble metals in particular have been discussed by numerous authors [1–3]. We give here a short account with emphasis on the classical pictures of the physical processes involved. The optical properties of metals can be described by a complex dielectric function that depends on the frequency of light (see Chapter 2). The properties are determined mainly by the facts that (i) the conduction electrons can move freely within the bulk of material and (ii) interband excitations can take place if the energy of the photons exceeds the bandgap energy of the respective metal. In the picture we adopt here, the presence of an electric field leads to a displacement $\mathbf{r}$ of an electron, which is associated with a dipole moment $\boldsymbol{\mu}$ according to $\boldsymbol{\mu} = e\mathbf{r}$. The cumulative effect of all individual dipole moments of all free electrons results in a macroscopic polarization per unit volume $\mathbf{P} = n\boldsymbol{\mu}$, where n is the number of electrons per unit volume. As discussed in Chapter 2, the macroscopic polarization $\mathbf{P}$ can be expressed as

$$\mathbf{P}(\omega) = \varepsilon_0 \chi_e(\omega)\mathbf{E}(\omega). \tag{12.1}$$

From (2.6) and (2.15) we have

$$\mathbf{D}(\omega) = \varepsilon_0 \varepsilon(\omega)\,\mathbf{E}\,(\omega) = \varepsilon_0 \mathbf{E}(\omega) + \mathbf{P}(\omega) \tag{12.2}$$

From this we calculate

$$\varepsilon(\omega) = 1 + \chi_e(\omega), \tag{12.3}$$

the frequency-dependent dielectric function of the metal. The displacement $\mathbf{r}$ and therefore the macroscopic polarization $\mathbf{P}$ and χ_e can be obtained by solving the equation of motion of the electrons under the influence of an external field.

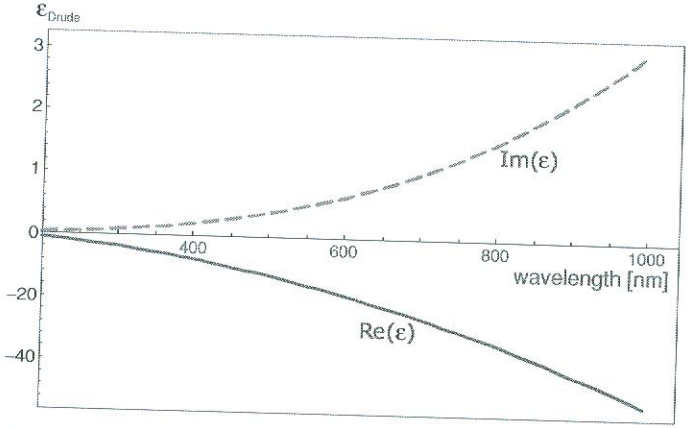

Figure 12.1 Real and imaginary part of the dielectric constant for gold according to the Drude–Sommerfeld free-electron model ($\hbar\omega_p = 8.95\,\text{eV}$, $\hbar\Gamma = 65.8\,\text{meV}$). The solid line is the real part, the dashed line is the imaginary part. Note the different scales for real and imaginary parts.

12.1.1 Drude–Sommerfeld theory

As a starting point, we consider only the effects of the free electrons and apply the Drude–Sommerfeld model for the free-electron gas (see e.g. [4]).

$$m_e \frac{\partial^2 \mathbf{r}}{\partial t^2} + m_e \Gamma \frac{\partial \mathbf{r}}{\partial t} = e\mathbf{E}_0 e^{-i\omega t}, \tag{12.4}$$

where e and m_e are the charge and the effective mass of the free electrons, and $\mathbf{E}_0$ and ω are the amplitude and the frequency of the applied electric field. Note that the equation of motion contains no restoring force since free electrons are considered. The damping term is proportional to $\Gamma = v_F/l$ where v_F is the Fermi velocity and l is the electron mean free path between scattering events. Solving (12.4) using the ansatz $\mathbf{r}(t) = \mathbf{r}_0 e^{-i\omega t}$ and using the result in (12.3) yields

$$\varepsilon_{\text{Drude}}(\omega) = 1 - \frac{\omega_p^2}{\omega^2 + i\Gamma\omega}. \tag{12.5}$$

Here $\omega_p = \sqrt{ne^2/(m_e\varepsilon_0)}$ is the volume plasma frequency. Expression (12.5) can be divided into real and imaginary parts as follows

$$\varepsilon_{\text{Drude}}(\omega) = 1 - \frac{\omega_p^2}{\omega^2 + \Gamma^2} + i\frac{\Gamma\omega_p^2}{\omega(\omega^2 + \Gamma^2)}. \tag{12.6}$$

Using $\hbar\omega_p = 8.95\,\text{eV}$ and $\hbar\Gamma = 65.8\,\text{meV}$, which are the values for gold, the real and the imaginary parts of the dielectric function (12.6) are plotted in Fig. 12.1 as a function of the wavelength over the extended visible range. We note that the real part of the dielectric constant is negative. One obvious consequence of this

behavior is the fact that light can penetrate a metal only to a very small extent since the negative dielectric constant leads to a strong imaginary part of the refractive index $n = \sqrt{\varepsilon}$. Other consequences will be discussed later. The imaginary part of ε describes the dissipation of energy associated with the motion of electrons in the metal (see Problem 12.1).

12.1.2 Interband transitions

Although the Drude–Sommerfeld model gives quite accurate results for the optical properties of metals in the infrared regime, it needs to be supplemented in the visible range by the response of bound electrons. For example for gold, at a wavelength shorter than ~550 nm, the measured imaginary part of the dielectric function increases much more strongly as predicted by the Drude–Sommerfeld theory. This is because higher-energy photons can promote electrons of lower-lying bands into the conduction band. In a classical picture such transitions may be described by exciting the oscillation of bound electrons. Bound electrons in metals exist e.g. in lower-lying shells of the metal atoms. We apply the same method that was used above for the free electrons to describe the response of the bound electrons. The equation of motion for a bound electron reads as

$$m\frac{\partial^2 \mathbf{r}}{\partial t^2} + m\gamma\frac{\partial \mathbf{r}}{\partial t} + \alpha \mathbf{r} = e\mathbf{E}_0 \mathrm{e}^{-\mathrm{i}\omega t}. \tag{12.7}$$

Here, m is the *effective* mass of the bound electrons, which is in general different from the effective mass of a free electron in a periodic potential, γ is the damping constant describing mainly radiative damping in the case of bound electrons, and α is the spring constant of the potential that keeps the electron in place. Using the same ansatz as before we find the contribution of bound electrons to the dielectric function

$$\varepsilon_{\text{Interband}}(\omega) = 1 + \frac{\tilde{\omega}_\mathrm{p}^2}{(\omega_0^2 - \omega^2) - \mathrm{i}\gamma\omega}\ . \tag{12.8}$$

Here $\tilde{\omega}_\mathrm{p} = \sqrt{\tilde{n}e^2/m\varepsilon_0}$ with $\tilde{n}$ being the density of the bound electrons. $\tilde{\omega}_\mathrm{p}$ is introduced in analogy to the plasma frequency in the Drude–Sommerfeld model, however, obviously here with a different physical meaning and $\omega_0 = \sqrt{\alpha/m}$. Again we can rewrite (12.8) to separate the real and imaginary parts

$$\varepsilon_{\text{Interband}}(\omega) = 1 + \frac{\tilde{\omega}_\mathrm{p}^2(\omega_0^2 - \omega^2)}{(\omega_0^2 - \omega^2)^2 + \gamma^2\omega^2} + \mathrm{i}\frac{\gamma\tilde{\omega}_\mathrm{p}^2\omega}{(\omega_0^2 - \omega^2)^2 + \gamma^2\omega^2}\ . \tag{12.9}$$

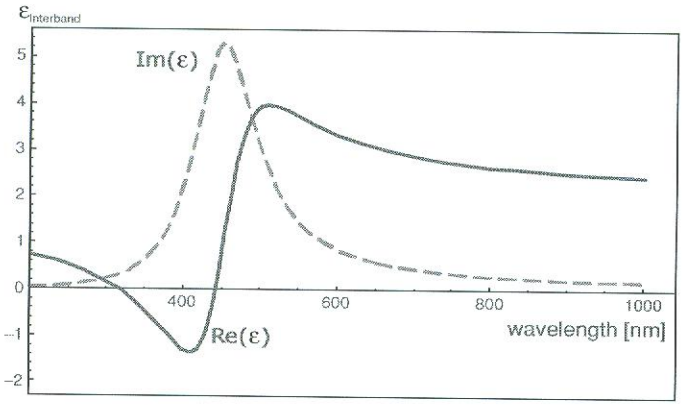

Figure 12.2 Contribution of bound electrons to the dielectric function of gold. The parameters used are $\hbar\tilde{\omega}_p = 2.96\,\text{eV}$, $\hbar\gamma = 0.59\,\text{eV}$, and $\omega_0 = 2\pi c/\lambda$, with $\lambda = 450\,\text{nm}$. The solid line is the real part, the dashed curve is the imaginary part of the dielectric function associated with bound electrons.

Figure 12.2 shows the contribution to the dielectric constant of a metal that derives from bound electrons.[1] Clear resonant behavior is observed for the imaginary part and dispersion-like behavior is observed for the real part. Figure 12.3 is a plot of the dielectric constant (real and imaginary part) taken from the paper of Johnson and Christy [5] for gold (open circles). For wavelengths above 650 nm the behavior clearly follows the Drude–Sommerfeld theory. For wavelengths below 650 nm obviously interband transitions become significant. One can try to model the shape of the curves by adding up the free-electron (Eq. (12.6)) and the interband absorption contributions (Eq. (12.9)) to the complex dielectric function (squares). Indeed, this much better reproduces the experimental data apart from the fact that one has to introduce a constant offset $\varepsilon_\infty = 6$ to (12.9), which accounts for the integrated effect of all higher-energy interband transitions not considered in the present model (see e.g. [6]). Also, since only one interband transition is taken into account, the model curves still fail to reproduce the data below ~500 nm.

12.2 Surface plasmon polaritons at plane interfaces

By definition surface plasmons are the quanta of surface-charge-density oscillations, but the same terminology is commonly used for collective oscillations in the electron density at the surface of a metal. The surface charge oscillations are naturally coupled to electromagnetic waves, which explains their designation as polaritons. In this section, we consider a plane interface between two media. One

[1] This theory naturally also applies for the behavior of dielectrics and the dielectric response over a broad frequency range consists of several absorption bands related to different electromagnetically excited resonances [2].

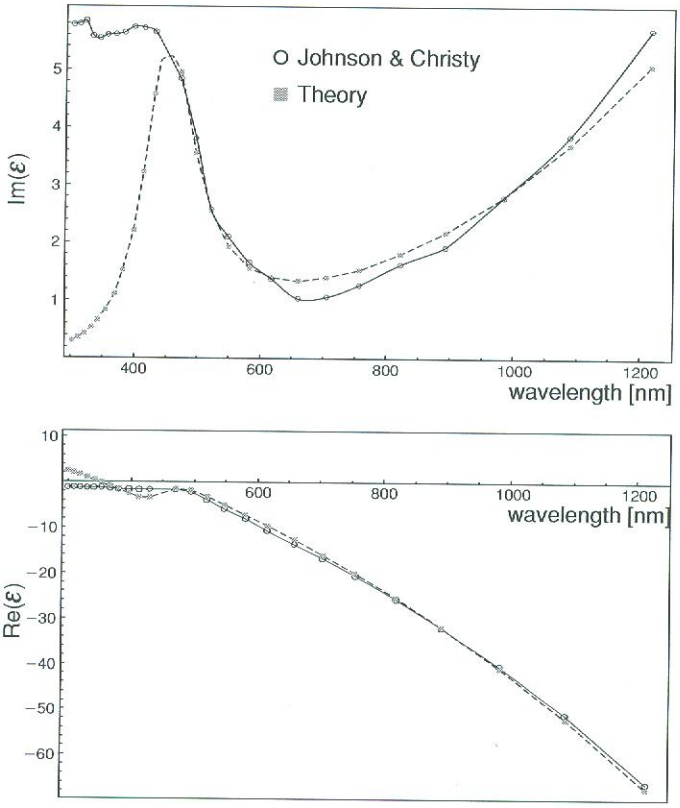

Figure 12.3 Dielectric function of gold: Experimental values and model. Upper panel: Imaginary part. Lower panel: Real part. Open circles: Experimental values taken from [5]. Squares: Model of the dielectric function taking into account the free-electron contribution and the contribution of a single interband transition. Note the different scales for the abscissae.

medium is characterized by a general, complex frequency-dependent dielectric function $\varepsilon_1(\omega)$ whereas the dielectric function of the other medium $\varepsilon_2(\omega)$ is assumed to be real. We choose the interface to coincide with the plane $z = 0$ of a Cartesian coordinate system (see Fig. 12.4). We are looking for *homogeneous* solutions of Maxwell's equations that are localized at the interface. A homogeneous solution is an eigenmode of the system, i.e. a solution that exists without external excitation. Mathematically, it is the solution of the wave equation

$$\nabla \times \nabla \times \mathbf{E}(\mathbf{r}, \omega) - \frac{\omega^2}{c^2} \varepsilon(\mathbf{r}, \omega)\, \mathbf{E}(\mathbf{r}, \omega) = 0\,, \tag{12.10}$$

with $\varepsilon(\mathbf{r}, \omega) = \varepsilon_1(\omega)$ if $z < 0$ and $\varepsilon(\mathbf{r}, \omega) = \varepsilon_2(\omega)$ if $z > 0$. The localization at the interface is characterized by electromagnetic fields that exponentially decay with increasing distance from the interface into both half-spaces. It is sufficient to

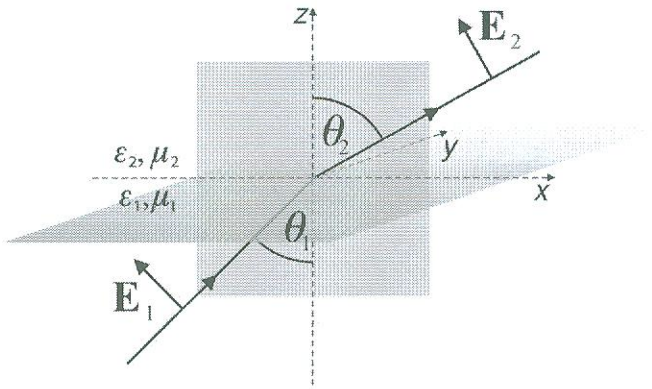

Figure 12.4 Interface between two media 1 and 2 with dielectric functions ε_1 and ε_2. The interface is defined by $z = 0$ in a Cartesian coordinate system. In each half-space we consider only a single p-polarized wave because we are looking for homogeneous solutions that decay exponentially with distance from the interface.

consider only p-polarized waves in both half-spaces because no solutions exist for the case of s-polarization (see problem 12.2).

p-polarized plane waves in half-spaces $j = 1$ and $j = 2$ can be written as

$$\mathbf{E}_i = \begin{pmatrix} E_{j,x} \\ 0 \\ E_{j,z} \end{pmatrix} \mathrm{e}^{\mathrm{i}k_x x - \mathrm{i}\omega t} \mathrm{e}^{\mathrm{i}k_{j,z} z}, \qquad j = 1, 2. \tag{12.11}$$

The situation is depicted in Fig. 12.4. Since the wavevector parallel to the interface is conserved (see Chapter 2) the following relations hold for the wavevector components

$$k_x^2 + k_{j,z}^2 = \varepsilon_j k^2, \qquad j = 1, 2\,. \tag{12.12}$$

Here $k = 2\pi/\lambda$, where λ is the vacuum wavelength. Exploiting the fact that the displacement fields in both half-spaces have to be source free, i.e. $\nabla \cdot \mathbf{D} = 0$, leads to

$$k_x E_{j,x} + k_{j,z} E_{j,z} = 0, \qquad j = 1, 2\,, \tag{12.13}$$

which allows us to rewrite (12.11) as

$$\mathbf{E}_j = E_{j,x} \begin{pmatrix} 1 \\ 0 \\ -k_x/k_{j,z} \end{pmatrix} \mathrm{e}^{\mathrm{i}k_{j,z} z}, \qquad j = 1, 2\,. \tag{12.14}$$

The factor $\mathrm{e}^{\mathrm{i}k_x x - \mathrm{i}\omega t}$ is omitted to simplify the notation. Equation (12.14) is particularly useful when a system of stratified layers is considered (see e.g. [7], p. 40 and Problem 12.4). While (12.12) and (12.13) impose conditions that define the fields

in the respective half-spaces, we still have to match the fields at the interface using boundary conditions. Requiring continuity of the parallel component of **E** and the perpendicular component of **D** leads to another set of equations which read as

$$\begin{aligned} E_{1,x} - E_{2,x} &= 0, \\ \varepsilon_1 E_{1,z} - \varepsilon_2 E_{2,z} &= 0. \end{aligned} \tag{12.15}$$

Equations (12.13) and (12.15) form a homogeneous system of four equations for the four unknown field components. The existence of a solution requires that the respective determinant vanishes. This happens either for $k_x = 0$, which does not describe excitations that travel along the interface, or for

$$\varepsilon_1 k_{2,z} - \varepsilon_2 k_{1,z} = 0\,. \tag{12.16}$$

In combination with (12.12), Eq. (12.16) leads to a dispersion relation, i.e. a relation between the wavevector along the propagation direction and the angular frequency ω,

$$k_x^2 = \frac{\varepsilon_1 \varepsilon_2}{\varepsilon_1 + \varepsilon_2} k^2 = \frac{\varepsilon_1 \varepsilon_2}{\varepsilon_1 + \varepsilon_2} \frac{\omega^2}{c^2}\,. \tag{12.17}$$

We also obtain an expression for the normal component of the wavevector

$$k_{j,z}^2 = \frac{\varepsilon_j^2}{\varepsilon_1 + \varepsilon_2} k^2, \qquad j = 1, 2. \tag{12.18}$$

Having derived (12.17) and (12.18) we are in a position to discuss the conditions that have to be fulfilled for an interface mode to exist. For simplicity, we assume that the imaginary parts of the complex dielectric functions are small compared with the real parts so that they may be neglected. A more detailed discussion that justifies this assumption will follow (see also [7]). We are looking for interface waves that propagate along the interface. This requires a real k_x.[2] Looking at (12.17) this can be fulfilled if the sum and the product of the dielectric functions are either both positive or both negative. In order to obtain a "bound" solution, we require that the normal components of the wavevector are purely imaginary in both media giving rise to exponentially decaying solutions. This can only be achieved if the sum in the denominator of (12.18) is negative. From this we conclude that the conditions for an interface mode to exist are the following:

$$\varepsilon_1(\omega) \cdot \varepsilon_2(\omega) < 0, \tag{12.19}$$

$$\varepsilon_1(\omega) + \varepsilon_2(\omega) < 0, \tag{12.20}$$

which means that one of the dielectric functions must be negative with an absolute value exceeding that of the other. As we have seen in the previous section, metals,

[2] Later we will see that by taking into account the imaginary parts of the dielectric functions k_x becomes complex, which leads to a damped propagation in the x-direction.

especially noble metals such as gold and silver, have a large negative real part of the dielectric constant along with a small imaginary part. Therefore, at the interface between a noble metal and a dielectric, such as glass or air, localized modes at the metal–dielectric interface can exist. Problem 12.3 discusses a possible solution for positive dielectric constants.

12.2.1 Properties of surface plasmon polaritons

Using the results of the previous section we will now discuss some properties of surface plasmon polaritons (SPP). To accommodate losses associated with electron scattering (ohmic losses) we have to consider the imaginary part of the metal's dielectric function [8]

$$\varepsilon_1 = \varepsilon_1' + \mathrm{i}\varepsilon_1'' \tag{12.21}$$

with ε_1' and ε_1'' being real. We assume that the adjacent medium is a good dielectric with negligible losses, i.e. ε_2 is assumed to be real. We then naturally obtain a complex parallel wavenumber $k_x = k_x' + \mathrm{i}k_x''$. The real part k_x' determines the SPP wavelength, while the imaginary part k_x'' accounts for the damping of the SPP as it propagates along the interface. This is easy to see by using a complex k_x in (12.11). The real and imaginary parts of k_x can be determined from (12.17) under the assumption that $|\varepsilon_1''| \ll |\varepsilon_1'|$:

$$k_x' \approx \sqrt{\frac{\varepsilon_1'\varepsilon_2}{\varepsilon_1' + \varepsilon_2}}\frac{\omega}{c}, \tag{12.22}$$

$$k_x'' \approx \sqrt{\frac{\varepsilon_1'\varepsilon_2}{\varepsilon_1' + \varepsilon_2}}\frac{\varepsilon_1''\varepsilon_2}{2\varepsilon_1'(\varepsilon_1' + \varepsilon_2)}\frac{\omega}{c}, \tag{12.23}$$

in formal agreement with Eq. (12.17). For the SPP wavelength we thus obtain

$$\lambda_{\mathrm{SPP}} = \frac{2\pi}{k_x'} \approx \sqrt{\frac{\varepsilon_1' + \varepsilon_2}{\varepsilon_1'\varepsilon_2}}\lambda \tag{12.24}$$

where λ is the wavelength of the excitation light in vacuum.

The propagation length of the SPP along the interface is determined by k_x'' which, according to (12.11), is responsible for an exponential damping of the electric field amplitude. The 1/e decay length of the electric field is $1/k_x''$ or $1/(2k_x'')$ for the intensity. This damping is caused by ohmic losses of the electrons participating in the SPP and finally results in a heating of the metal. Using $\varepsilon_2 = 1$ and the dielectric functions of silver ($\varepsilon_1 = -18.2 + 0.5\mathrm{i}$) and gold ($\varepsilon_1 = -11.6 + 1.2\mathrm{i}$) at a wavelength of 633 nm, we obtain 1/e intensity propagation lengths of the SPP of $\sim$60 μm and $\sim$10 μm, respectively. The decay length of the SPP electric fields